Available online at www.sciencedirect.com
ScienceDirect
European Journal of Pharmaceutics and Biopharmaceutics 69 (2008) 72–82
European Journal of Pharmaceutics and Biopharmaceutics
www.elsevier.com/locate/ejpb

Research paper

Developing an environmentally benign process for the production of microparticles: Amphiphilic crystallization

Darragh Murnane, Christopher Marriott, Gary P. Martin *

King's College London, Pharmaceutical Science Research Division, London, United Kingdom

Received 17 July 2007; accepted in revised form 24 October 2007
Available online 1 November 2007

Abstract

The production of microparticles for inhalation typically employs jet-milling which can be destructive to the solid-state properties of the particles. The objective of the current work was to develop a crystallization process for the production of respirable microparticles of salmeterol xinafoate (SX) with a controlled particle size distribution (PSD). Solvation of SX in aqueous poly(ethylene glycol) 400 (PEG 400) was investigated using HPLC and FTIR. SX was crystallized from PEG 400 solutions by the addition of water under a variety of conditions of supersaturation, addition rate of antisolvent and stirring speed. The crystals were filtered, dried at 50 °C and their PSDs were determined by laser diffraction. A logarithmic increase in solubility of SX was observed with increasing concentration of PEG 400 in water enabling the aqueous antisolvent crystallization of SX from PEG. Similar to antisolvent crystallization from conventional solvents, a 2^4 factorial study showed the particle size to decrease with increasing supersaturation. The PSD also depended on the balance of meso- and micromixing determined by the crystallization conditions. In particular a high addition rate (200 g min^{-1}) and low stirrer speed (400 rpm) minimized the median diameter (2.54 ± 0.40 μm) and produced a narrow PSD ($90\% < 8.67 \pm 0.77$ μm) of SX particles. Amphiphilic crystallization provided a novel, environmentally benign method to produce microparticles of SX with a controlled size range.

Keywords: Crystallization; Antisolvent micronization; Factorial design; Poly(ethylene glycol); Salmeterol xinafoate

1. Introduction

The topical delivery of aerosols containing an active pharmaceutical ingredient (API) such as corticosteroids and bronchodilators directly to the airways maximizes the locally produced pharmacological effect of the API whilst potentially limiting systemic exposure and the resultant side effects. There is also an increasing interest in exploiting the large absorptive potential of the alveolar epithelium for the systemic delivery of drug substances, particularly macromolecules [1,2]. This has culminated in the recent regulatory approval of inhaled human insulin for the therapy of diabetes [3].

The aerodynamic diameter of the dispersed droplets or particles is the principal determinant of effective pulmonary deposition of therapeutic aerosols. For effective localized/topical therapy of obstructive lung diseases an aerodynamic particle size of 2.5–6 μm is required [4]. Particles of APIs in this size range display poor flow properties [5,6] and are highly cohesive/adhesive. The above combination makes filling of powders into inhalation devices complex and irreproducible and the formation of a de-aggregated aerosol cloud is difficult. To aid delivery of the API, micron-sized particles can be formulated with propellants as a pressurized metered dose inhaler (MDI) formulation. Alternatively such particles can be agglomerated into pellets or blended to form an ordered mixture with a coarse carrier such as lactose in a dry powder inhaler (DPI) formulation and device combination [7].

* Corresponding author. King's College London, Drug Delivery Research Group, Pharmaceutical Science Research Division, 150 Stamford Street, London SE1 9NH, United Kingdom. Tel.: +44 (0)20 7848 4791; fax: +44 (0)20 7848 4800.
E-mail address: gary.martin@kcl.ac.uk (G.P. Martin).

0939-6411/$ - see front matter © 2007 Elsevier B.V. All rights reserved.
doi:10.1016/j.ejpb.2007.10.014

Typically only 10–20% of the labelled dose of API is deposited in the lung from an MDI aerosol, whilst that from passive DPIs ranges from 5.5% to 28.8%, with the latter generally demonstrating higher variability [8]. Patients often experience difficulties using devices effectively and this contributes to low pulmonary deposition and poor clinical outcomes [9,10]. Low pulmonary deposition also results, however, from deficiencies in the MDI [11] and DPI [12,13] aerosol formulations themselves. For example, variable and low *in vitro* emitted doses have been reported from DPI formulations [14]. This is symptomatic of high particle retention in devices and the adhesion of API to carrier particles because forces of particulate cohesion and adhesion must be overcome to produce a respirable aerosol cloud.

Particles in the size range 1–10 μm are traditionally produced by the crystallization of macrocrystals of the drug substance followed by a subsequent micronization step. Micronization is a high energy size-reduction process, typically performed in an air-jet mill, which exerts poor control over particle size, shape and size distribution [7]; all of which influence the aerodynamic properties of particles [15]. Micronization of API crystals has been demonstrated to introduce amorphous character into the resultant particles as a result of a solid-state transition to a metastable phase [16–19]. Polymorphic transitions have also been reported to result from milling processes [20,21] and an alteration in particle surface energy has been measured following milling [22–25].

Despite its widespread use, micronization is an undesirable production technique for respirable particles. The disturbances in surface crystallinity and surface energization can affect the adhesive/cohesive forces between micronized particles of APIs and other formulation components [26]. The energization of surfaces has resulted in blends lacking homogeneity [27]; it affects the physical stability of DPI and MDI formulations [28–30]; and it can affect the aerosolization of API particles from DPI formulations [6,31]. Alternative production techniques falling under the banner of 'particle engineering' have been developed to overcome such deficiencies of the macrocrystallization and micronization approach for the production of respirable particles (see recent technology reviews by Chan and Chew [7] and Chow et al. [32]).

Precipitation by antisolvent crystallization represents an attractive constructive approach for the production or respirable particles and may be termed antisolvent micronization. Precipitation is a rapid crystallization process characterized by high levels of solute supersaturation, generated upon the homogeneous mixing of a solution of an API with an appropriate antisolvent. Generating a molecularly homogeneous solvent composition throughout the crystallizer prior to nucleation is difficult at high supersaturation [33] resulting in disperse crystal nucleation and growth rates throughout the crystallizer [7]. Agglomeration and aging of precipitates may broaden the particle size distribution (PSD) yet further [34]. Control of the PSD is consequently difficult, as are reproducible generation of particles and scale up of the crystallization process.

Strategies to control the PSD by limiting crystal growth and agglomeration during precipitation include the use of crystal growth inhibiting polymers [35–37]; the use of controlled mixing technologies [38,39]; the application of ultrasound to accelerate diffusion and nucleation [40,41]; and the use of supercritical fluid antisolvent technologies [32]. These approaches, however, demonstrate several major deficiencies as process technologies. First, the presence of polymeric stabilizing excipients in the final API-containing particles is undesirable. Second, the presence of polymeric stabilizers on the surface of the particles contributes to amorphous content [36], although crystallization techniques are intended to avoid the generation of amorphous regions during milling. Third, the use of growth inhibitors is highly specific for the molecule being crystallized and is also concentration dependent. All these factors result in further complications when developing an appropriate crystallization process. In addition, in the case of hydrophobic APIs such approaches require the use of potentially harmful organic solvents.

The use of conventional solvents in the pharmaceutical industry requires careful handling procedures during processing to avoid combustion and exposure for operators. The use of organic solvents also necessitates their thorough removal from the final product and questions can remain over the presence of residual solvents, even when using supercritical fluid techniques [42]. The use of poly(ethylene glycol) (PEG) in place of conventional solvents represents an attractive alternative since appropriate grades of the polymer display good solubility in water and in non-polar solvents. The amphiphilic polymer demonstrates notable powers of aqueous solubilization for hydrophobic drug molecules [43]. PEG has been proposed as a safe solvent because it demonstrates low flammability, low toxicity and it is non-volatile [44]. Thus the difficulties in using conventional organic solvents for pharmaceutical processing are obviated. An additional rationale for employing PEG as an alternative solvent is the polymer's biodegradability [45,46] which renders it environmentally benign, in comparison to conventional solvents. PEG is also on the Food and Drug Administration's 'generally regarded as safe (GRAS)' list.

Aqueous solutions of PEG are used in the crystallization and recovery of proteins [47,48], including the pharmaceutically relevant protein interferon alpha-2a [49]. Most recently low molecular weight PEGs have been explored as a crystallization medium for macrocrystals of small molecular weight species [50]. Despite the latter observation and the use of PEG as a solvent for production of macrocrystals, the feasibility of using PEG for the production of microparticles has yet to be investigated. Propylene glycol represents an alternative non-volatile solvent for antisolvent techniques [51], however, it was shown that similar to conventional organic solvents, macrocrystals were produced unless a crystal growth inhibitor (HPMC) was included [52]. Microfine suspensions of API crystals

have been generated upon dissolution of high molecular weight PEG solid dispersions [53]. Therefore, both high and low molecular weight PEGs provide interesting novel solvent systems worthy of investigation for the antisolvent micronization of pharmaceuticals.

PEG has been employed in experimental dry powder [54] and metered dose inhaler [55] formulations but the toxicity of PEG delivered by pulmonary administration requires investigation [56,57]. However, it was not the intention of the current study to produce formulations containing PEG. The aim of this work was to investigate and develop an amphiphilic crystallization (AmphiCrys) process comprising PEG–water crystallization systems for the antisolvent micronization of particles of API generated for topical lung delivery. In order to understand the manufacturing parameters controlling the crystal size distribution, factorial design of experiments was employed.

2. Materials and methods

2.1. Materials

PEG 400, Analar® grade cyclohexane and HiPerSolv® grade ammonium acetate were purchased from BDH (VWR International Ltd., Poole, UK). High performance liquid chromatography grade methanol was purchased from Fisher Scientific Ltd. (Loughborough, UK) or from VWR International Ltd. (Poole, UK). An Inertsil® ODS 2 column (5 μm, 200 × 4.6 mm i.d.) was obtained from Capital HPLC Ltd. (Broxburn, UK). Span 80 was purchased from Sigma–Aldrich Company Ltd. (Gillingham, UK). Nylon filters (0.45 μm pore size, 47 mm diameter) and cellulose acetate syringe filters (0.45 μm pore size, Schleicher and Schuell brand) were obtained from Whatman Intl. Ltd. (Maidstone, UK). Water was produced by reverse osmosis using an ElgaStat unit (Elga LabWater, Marlow, UK). Silica gel was purchased from Prolabo (VWR International Ltd., Poole, UK). Salmeterol xinafoate (SX) was a generous gift from GlaxoSmithKline Pharmaceutical Development (Ware, UK).

2.2. Determination of the equilibrium solubility of salmeterol xinafoate

PEG 400 solutions in water were prepared by weighing appropriate amounts of PEG into volumetric flasks. Water was added to the PEG to produce a series of weight/weight solutions (range 0–100% w/w PEG 400). The solutions were mixed using a magnetic stirrer plate and follower (IKA Werke GmbH and Co. KG, Staufen, Germany). Each solution was transferred in turn to a glass beaker and excess SX was added. These suspensions were stirred for 5 min at 7000 rpm using a Silverson L4RT Mixer with a high shear square hole head (Silverson Machines Ltd., Chesham, UK). Aliquots of the suspensions were transferred to glass vials, to which excess drug was added together with a magnetic flea and the vials were sealed. The suspensions were ultrasonicated (Decon FS300B Bath, Decon Laboratories Ltd., Hove, UK) for 40 min to aid dispersion and dissolution. The suspensions were then placed on a multiplate Variomag® stirrer (H+P Labortechnik Ag., Oberschleissheim, Germany), and were left to equilibrate for 72 h at 25 °C in a temperature controlled water bath (Grant SSD40, Grant Instruments, Chelmsford, UK).

Samples were filtered through 0.45 μm cellulose acetate syringe filters into volumetric flasks, which were then weighed. Alternatively, for higher concentrations of PEG, samples were centrifuged at 16,060*g* for 5 min (Biofuge pico, Heraeus, Kendro Laboratory Products plc, Bishops Stortford, UK) and the supernatant was transferred into volumetric flasks and weighed. Samples were diluted appropriately with mobile phase, and analyzed for drug content by high performance liquid chromatography (HPLC) according to a validated HPLC assay for SX [58] employing a HP1090 integrated HPLC system with a HP1050 variable wavelength detector (Agilent Technologies UK Ltd., Wokingham, UK). All other chromatographic conditions were as reported previously [58] and calibration curves were prepared for each fresh batch of mobile phase using calibration standards in the range 1–100 μg mL^{-1} SX in mobile phase.

2.3. Particle size determination

Particle sizing was carried out by laser diffraction using the Malvern Mastersizer X (Malvern Instruments Ltd., Malvern, UK) equipped with a 100 mm focal length lens and an MS7 magnetically stirred cell using the 2 NHE software presentation. The sizing methods were validated according to ISO 13320 (1990) standards to demonstrate fitness for purpose (data not presented). SX-saturated solutions of 0.5% w/v Span 80 in cyclohexane were prepared by sonicating the dispersant solution with an excess of drug for 60 min, followed by stirring overnight with a magnetic follower. The saturated dispersant solution was filtered through 0.45 μm cellulose acetate syringe filters into the sample cell of the Malvern Mastersizer. The crystals of SX (approximately 1 mg) were added to an 8 mL glass vial and 2 mL of filtered dispersant was added. The suspension was sonicated in a water bath for 5 min (Sonicleaner, Dawe Ultrasonics Ltd., USA) to allow dispersion of the particles and aliquots were added successively to the sample cell by means of a Gilson pipette to achieve a satisfactory obscuration level (20% obscuration) and allowed to equilibrate for 60 s. At least three measurements were taken with each batch of crystals, samples being taken from different locations in the powder bed. Each individual sample was measured five times using 2500 measurement sweeps at a stirrer speed of 3 scale units.

2.4. Crystallization of salmeterol xinafoate

2.4.1. Preparation of SX in PEG 400 solutions

Solutions of SX were prepared by weighing the appropriate amount into a glass beaker and adding sufficient

PEG 400 to achieve the required concentration (% w/w). The beakers were covered with sealing film, and the solution was subjected to ultrasonication at 400 W and 40 kHz (Decon FS300B bath, Decon Laboratories Ltd., Hove UK) for 5 min to aid SX dispersion and dissolution. Thereafter the solutions were mixed using a Silverson L4RT Mixer with 1″ tubular frame rod and a high shear square hole head according to the following protocol: 2000 rpm for 10 min, 3000 rpm for 10 min, 1000 rpm for 5 min and finally ultrasonication for 5 min to degas. The solutions were then filtered using a 0.45 μm cellulose acetate syringe filter into glass vials and sealed.

2.4.2. Infrared analysis of PEG solutions

Solutions of SX in PEG 400 were analyzed by attenuated total reflectance Fourier transform infrared spectroscopy (ATR-FTIR). FTIR spectra were recorded using a Spectrum One spectrometer and spectral analysis was performed with Spectrum version 5.3.1 software (Perkin Elmer (UK) Ltd., Beaconsfield, UK). The solutions were analyzed using the Spectrum One HATR Zinc Selenide (ZnSe) 45° ATR crystal trough plate. Samples were scanned 32 times over the 450–4000 cm^{-1} range with a resolution of 4 cm^{-1}.

2.4.3. Crystallization by antisolvent addition

The PEG solution was weighed into a standard 250 mL glass beaker (diameter = 70.0 mm). The beaker was placed on a laboratory elevator platform, under a Eurostar digitally controlled overhead stirrer (IKAwerk GmbH and Co. KG, Staufen, Germany) equipped with a stainless steel four blade turbine-propeller stirrer (cross-section 4 cm). The platform together with the beaker was raised, such that the propeller was positioned precisely at the centre. The vertical position of the stirrer was such that the underside of the stirrer was directly above the base of the beaker, but not in contact with the glass.

Water was added as the antisolvent at a controlled rate using a model 505S peristaltic pump (Watson Marlow Bredel Pumps Ltd., Falmouth, UK) equipped with 6 mm internal diameter silicon tubing, which had a 2 mm thick wall. A 1 mL plastic Gilson pipette tip fixed to the end of the silicon tubing was used to direct the water flow. The antisolvent was directed to flow down the side wall of the glass beaker allowing initial contact with the surface of the PEG solution at the beaker wall. The pump was calibrated for each desired flow rate, to ensure the addition of the correct weight of reverse osmosis water (filtered through a 0.45 μm nylon membrane). The time for the addition of water differed randomly from batch to batch, depending upon the amount of PEG solution initially weighed into the beaker.

The crystals were harvested by vacuum filtration using a 0.45 μm nylon membrane filter (47 mm diameter) housed in a glass filter unit (Millipore (UK) Ltd., Watford, UK). The wet cake was washed with 2× 100 mL volumes of water; the latter having been filtered through a 0.45 μm nylon filter and pre-cooled to 4 °C. The washed filter cakes were transferred to Petri dishes, covered with perforated aluminium foil, and dried *in vacuo* at 50 °C overnight (Vacutherm, Heraeus GmbH, Hanau, Germany). The dry cake was transferred to sealed glass vials and stored at room temperature over dried silica gel in a glass desiccator.

2.4.4. Experimental design for screening the effects of crystallization conditions

A 2^4 (two-level four factor) full-factorial experiment was designed using Design-Expert 5.0 software (StatEase, QD Consulting, Penzance, UK). SX was crystallized from

Table 1
Combinations of the operational variables investigated in the antisolvent crystallization of salmeterol xinafoate from PEG 400–water and the resultant particle size distribution of the crystals (particle sizes represent mean ± SD, $n = 3$ determinations, except *, $n = 1$)

Experiment No.	Standard order No.	SX conc. (% w/w)	PEG conc. (% w/w)	Stirrer speed (rpm)	Addition rate (g min^{-1})	$D_{(v,0.1)}$ (μm)	$D_{(v,0.5)}$ (μm)	$D_{(v,0.9)}$ (μm)	Yield (%)
1	10	6.00	1.00	300	200.0	1.82 ± 0.27	7.85 ± 0.65	16.43 ± 1.14	47.95
2	8	6.00	10.00	2000	5.0	0.75 ± 0.02	5.03 ± 0.48	29.09 ± 2.10	57.45
3	19	3.50	5.50	1150	102.5	0.64 ± 0.00	3.06 ± 0.12	11.33 ± 0.70	55.80
4	7	1.00	10.00	2000	5.0	0.72 ± 0.02	4.44 ± 0.50	20.13 ± 0.61	46.52
5	4	6.00	10.00	300	5.0	0.70 ± 0.03	4.59 ± 0.58	32.70 ± 4.11	67.54
6	6	6.00	1.00	2000	5.0	0.77 ± 0.03	8.22 ± 2.42	43.65 ± 8.98	51.26
7	16	6.00	10.00	2000	200.0	0.67 ± 0.02	4.07 ± 0.64	37.49 ± 5.94	65.75
8	5	2.00	1.00	2000	5.0	0.78 ± 0.02	5.84 ± 0.29	34.38 ± 1.96	34.61
9	3	1.00	10.00	300	5.0	0.90 ± 0.15	5.32 ± 1.46	11.96 ± 2.83	50.99
10	17	3.50	5.50	1150	102.5	0.63 ± 0.01	2.98 ± 0.09	15.05 ± 0.51	49.76
11	11	1.00	10.00	300	200.0	1.34 ± 0.24	8.38 ± 0.63	17.94 ± 0.99	43.52
12	1	2.00	1.00	300	5.0	0.70 ± 0.06	3.70 ± 0.87	23.74 ± 1.28	31.28
13	13	2.00	1.00	2000	200.0	1.03 ± 0.08	14.98 ± 0.73	34.93 ± 0.40	20.01
14	18	3.50	5.50	1150	102.5	0.63 ± 0.02	2.62 ± 0.27	11.40 ± 1.38	53.62
15	14	6.00	1.00	2000	200.0	0.75 ± 0.02	6.33 ± 0.84	28.95 ± 4.07	37.08
16*	9	2.00	1.00	300	200.0	2.84	11.62	23.32	0.30
17	2	6.00	1.00	300	5.0	0.67 ± 0.02	3.65 ± 0.49	31.55 ± 4.02	49.14
18	12	6.00	10.00	300	200.0	0.75 ± 0.02	4.11 ± 0.29	10.54 ± 0.50	65.22
19	15	1.00	10.00	2000	200.0	0.89 ± 0.08	6.34 ± 0.89	21.60 ± 2.46	41.46

PEG 400 solutions according to the general method presented above. The final weight of the crystallization solutions was ~170 g, such that the initial weights of PEG solutions varied from 1.6 to 19.1 g. The factors considered were SX concentration in the PEG solution, final concentration of PEG in the crystallizing solution, stirrer speed and the addition rate of the antisolvent. The details of the factor levels employed for the crystallization experiments are presented in Table 1. The response factor examined was the volume median diameter ($D_{(v,0.5)}$) of the resultant crystallized SX as measured by laser diffraction. Runs 8, 12, 13 and 16 required a deviation (2% w/w) from the low factor of SX concentration (1% w/w) in PEG 400, as there was no particle output at the 1% w/w level. Crystallization was terminated 20 min after the full addition of the antisolvent, and percentage yields were calculated using the following equation:

$$\text{Yield} = \frac{\text{mass dried SX} \times 100}{(\text{Mass SX/PEG solution employed}) \times (\text{conc. of SX/PEG solution})} \quad (1)$$

2.4.5. Experimental design for the optimization of crystallization conditions

A 3^2 full-factorial study was carried out using the centre point from the 2^4 full-factorial study as the centre point. The factors investigated were stirrer speed and antisolvent addition rate, with both SX in PEG 400 (3.5% w/w) concentration and the solution to antisolvent ratio held constant (5.5% w/w PEG). The stirrer speeds investigated were 400, 1200 and 2000 rpm. The addition rate of water was studied at 10, 100.5 and 200 g min^{-1}. In all cases the weight of the PEG solution was 8 g and the final weight of the crystallization medium was 140 g.

3. Results

3.1. Solubilization of salmeterol xinafoate by PEG 400

To investigate the suitability of PEG 400 as a crystallizing solvent for the antisolvent micronization of SX it was necessary to establish the solubilization capacity of aqueous PEG for SX. A logarithmic increase in the solubility of SX with increasing concentration of PEG in water was achieved (Fig. 1). The plot of logarithm of the solubility (S) of SX displayed a linear relationship with PEG concentration ($r^2 = 0.991$). The regression equation for the solubility in the cosolvent system was

$$\text{Log10}S = 0.0335(\pm 0.0004)\text{PEGconc} + 1.736(\pm 0.022) \quad (2)$$

However, the regression analysis revealed a significant lack of fit ($p < 0.001$), which was attributed to the deviation from linearity between 90% w/w and 100% w/w PEG 400 in water.

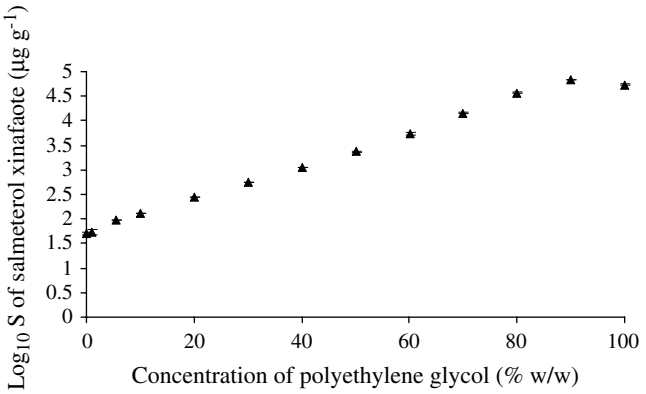

Fig. 1. The Log_{10} solubility (S) of salmeterol xinafoate as a function of the weight fraction of PEG 400 (▲) (each data point represents the mean ± SD, $n \geqslant 3$).

SX dissolved in PEG 400 caused a change in the FTIR spectrum of PEG 400 (Fig. 2A). A change in the OH stretching vibrational bands centred around 3400 cm^{-1} was observed. Further changes were observed in the methylene rocking, bending and wagging region of PEG between 1350 and 1700 cm^{-1} (Fig. 2B). The peak at 1415 cm^{-1} (CH_2 wagging and twisting) and shoulder at 1434 cm^{-1} (CH_2 wagging) both increased in intensity as a function of SX concentration. Peaks at 1350 cm^{-1} (CH_2 wagging and CC stretching) and 1280 cm^{-1} (CH_2 twisting) were found to broaden in the presence of SX. Two peaks (1615 and 1583 cm^{-1}) attributable to NH_2^+ deformation and CO_2^- salt deformation for SX were observed to increase in intensity with SX concentration in PEG.

3.2. Screening factorial experimental design

A 2^4 full-factorial design was used to screen the effects of four key crystallization conditions on the potential to produce microparticles of SX which may be suitable for inhaled delivery. Table 1 presents the input conditions of crystallization, the resulting particle size distribution and actual drug crystal yield of SX microparticles. The median diameter of the standard micronized material used as the raw material was 1.13 ± 0.12 μm, with a cumulative 90% undersize of 3.69 ± 0.23 μm.

Experiments 3, 10 and 14 represent the centre point conditions which were investigated to detect curvature in the response surface. Crystallizing SX in three separate experiments according to the centre point conditions allowed the determination of the reproducibility of the crystallization process. There was no significant difference between the mean cumulative 10% undersize ($D_{(v,0.1)}$) or median diameter ($D_{(v,0.5)}$) values for any of the three batches (ANOVA $p = 0.357$ and $p = 0.053$, respectively). This demonstrated a greater degree of variance arising from the determination of median particle size (the primary response for the factorial study) than that which arose from the crystallization process. A significant difference was observed for the

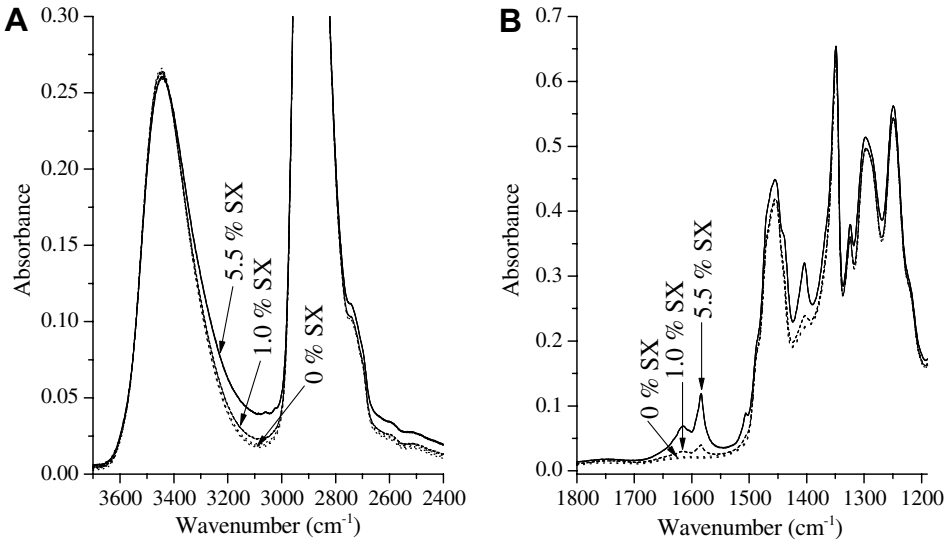

Fig. 2. The hydroxyl and methylene stretching regions (A) and the methylene deformation region (B) of the infrared spectra (ATR-FTIR) of PEG 400 and of salmeterol xinafoate dissolved in PEG 400 at 1.0% w/w and 5.5% w/w.

cumulative 90% undersize values ($D_{(v,0.9)}$) for the three replicates (ANOVA $p > 0.05$).

It was clear from the particle size data in Table 1 that the crystallization process was successful in producing crystals in the low micron size range, which would be suitable for process optimization. The range of median diameter values was 2.62 ± 0.27 to 14.98 ± 0.73 μm while the cumulative 90% undersize values ranged from 10.54 ± 0.50 to 43.65 ± 8.98 μm. This demonstrated that the factors studied did indeed have an effect on the properties of the crystallized drug.

The median diameter data were analyzed statistically using Design Expert 5.0 software without carrying out any transformation of the data. The input factors having a significant effect were coded alphabetically (e.g. A = drug concentration), while interactions were represented by combinations (e.g. AB = drug concentration and PEG concentration interaction). The model was constructed by step-wise backward elimination of statistically insignificant factorial terms and non-hierarchical terms (e.g. ACD was removed because the AC interaction was insignificant). The final model is presented in Table 2 along with the regression coefficients which are a measure of the magnitude of the effect of a factor on the median diameter of SX microparticles produced by aqueous antisolvent crystallization from PEG 400. A statistical analysis of variance of the model is presented in Table 3. Briefly, although the model was significant ($p < 0.0001$) as indicated by its ability to account for 85% of the variance in the $D_{(v,0.5)}$ (adjusted R-squared = 0.849), there was a significant lack of fit to the data ($p < 0.0001$) principally arising from the presence of curvature ($p < 0.0001$) in the response surface.

Table 2
Regression analysis of the factorial model of the median diameter of salmeterol xinafoate particles crystallized in a two-level, four factor full-factorial study, detailing the statistical significance and relative magnitude of the factorial response coefficients

Factor	Coefficient estimate	Standard error	$p > \|t\|$
Intercept	6.82	0.16	<0.0001
A = drug concentration (% w/w)	−1.24	0.18	<0.0001
B = PEG concentration (% w/w)	−1.53	0.16	<0.0328
C = stir rate (rpm)	0.35	0.16	<0.0001
D = addition rate (g min^{-1})	1.72	0.17	<0.0366
AB	0.40	0.18	<0.0001
AD	−1.71	0.18	<0.0002
BC	−0.67	0.16	<0.0001
BD	−1.27	0.17	<0.0018
CD	−0.53	0.16	<0.0001
ABD	0.91	0.18	<0.0001
Centre point	−3.93	0.39	<0.0001

3.3. Response surface construction to optimize crystallization parameters

From the particle sizing data presented in Table 4, it is clear that the two operating conditions of stirrer speed and addition rate of the antisolvent affected the PSD of the microcrystals. It was possible to decrease the median diameter of the particles to a size suitable for inhalation drug delivery, and also to narrow the particle size distribution by decreasing the cumulative 90% undersize diameter. The median diameters ranged from 2.42 ± 0.42 to 4.97 ± 1.01 μm, while the 90% undersize diameter ranged from as low as 8.67 ± 0.77 μm to as large as 32.98 ± 6.55 μm.

It was necessary to include two forced terms (stir rate and stir rate–addition rate interaction) to retain hierarchy of the response surface model for the median diameter and to improve the statistical fit. No forced terms were necessary for the $D_{(v,0.9)}$ response surface model. The response surfaces for the particle size distribution are presented in Figs. 3 and 4, both of which indicate a quadratic curvature term, while the analyses of variance and model regressions

Table 3
Summary of the analysis of variance for the model equation of the median diameter of salmeterol xinafoate particles as a function of the crystallization variables

Source	Sum of squares	DF	Mean square	F value	$p > F$
Model	337.49	10	33.749	30.184	<0.0001
Curvature	114.26	1	114.260	102.190	<0.0001
Residual	46.961	42	1.1181		
Lack of fit	31.655	5	6.331	15.305	<0.0001
Pure error	15.306	37	0.4137		
Root mean square error		1.057	R-squared		0.878
Dependent mean		5.755	Adjusted R-squared		0.849
% Coefficient variance		18.375	Predicted R-squared		0.826
Predicted residual sum squares		86.937	Adequate precision		23.063

Table 4
Particle size distribution by laser diffraction for particles of salmeterol xinafoate crystallized according in a 3^2 factorial study (mean ± SD, $n = 5$)

Stirrer rate (rpm)	Addition rate (g min^{-1})	$D_{(v,0.1)}$ (μm)	$D_{(v,0.5)}$ (μm)	$D_{(v,0.9)}$ (μm)
400	10.0	0.75 ± 0.06	4.97 ± 1.01	18.85 ± 3.12
400	100.5	0.70 ± 0.02	3.84 ± 0.52	9.80 ± 1.17
400	200.0	0.64 ± 0.02	2.54 ± 0.40	8.67 ± 0.77
1200	10.0	0.69 ± 0.02	4.23 ± 0.49	32.98 ± 6.55
1200	100.5	0.65 ± 0.01	3.00 ± 0.30	10.02 ± 0.94
1200	200.0	0.64 ± 0.02	2.42 ± 0.42	8.93 ± 0.69
2000	10.0	0.79 ± 0.03	4.60 ± 0.19	23.53 ± 3.84
2000	100.5	0.66 ± 0.01	3.46 ± 0.32	23.57 ± 1.86
2000	200.0	0.64 ± 0.01	3.19 ± 1.06	21.74 ± 2.63

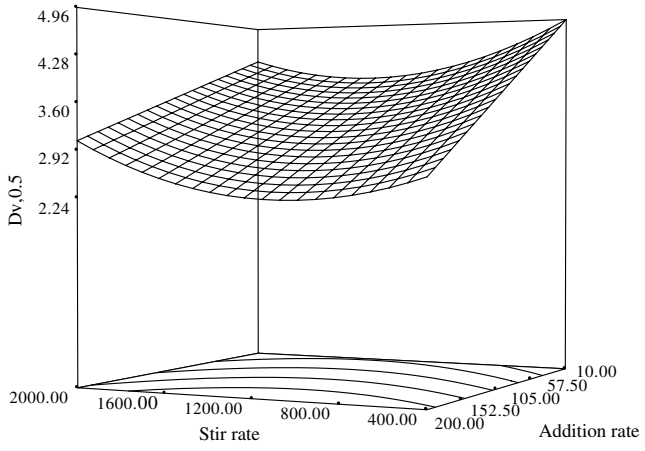

Fig. 3. Response surface demonstrating the effects of the stirrer speed (rpm) and antisolvent addition rate (g min^{-1}) on the median diameter ($D_{(v,0.5)}$, μm) of salmeterol xinafoate particles.

are presented in Tables 5 and 6. The median diameter was dependent on all terms included in the model response surface for the $D_{(v,0.5)}$ ($p < 0.0001$) and no significant lack of fit was displayed. The response surface, however, was not suitable for the predictive optimization experiments outside the experimental space (adjusted correlation coefficient = 0.654). Although the model for the $D_{(v,0.9)}$ response surface described the data well ($p < 0.0001$), a significant lack of fit was observed ($p < 0.0001$) as confirmed by the lower correlation coefficient (adjusted R-squared = 0.654).

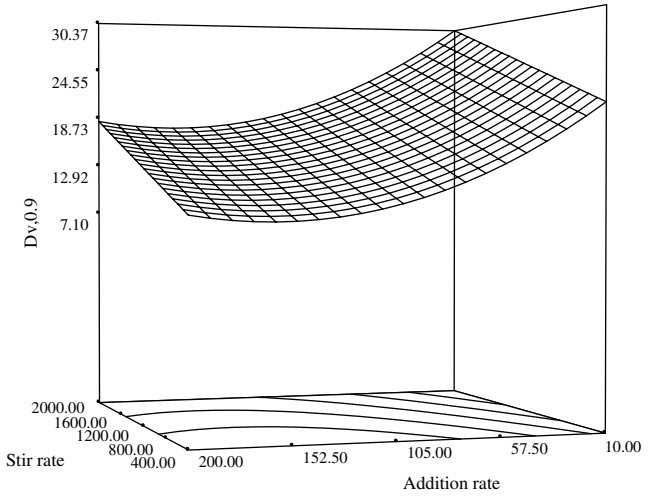

Fig. 4. Response surface demonstrating the effects of the stirrer speed (rpm) and the antisolvent addition rate (g min^{-1}) on the cumulative 90% undersize diameter ($D_{(v,0.9)}$, μm) of salmeterol xinafoate particles.

4. Discussion

The generation of solution supersaturation is the driving force for solute precipitation in antisolvent micronization processes. Establishing the feasibility of controlled precipitation requires a thorough knowledge of the equilibrium solubility of the crystallizing substance as a function of antisolvent concentration. Only if a significant difference exists between the solubility of the substance in the solvent and antisolvent can a precipitation process be effective.

PEG 400 solubilized SX with a typical log-linear increase in solubility [59] as PEG concentration increased. There is an approximately 1000-fold difference between the solubility of SX in pure PEG 400 and in pure water. The deviation from log-linearity at high fractions of cosolvent is not uncommon [60] and is usually observed in non-ideal solutions where specific solvation interactions exist (e.g. H-bonding). Solutions of PEG in water show extensive interactions in the form of intermolecular H-bonds [61] which break down the structure of water [62] and hence facilitate an increase in solubility of hydrophobic compounds such as SX. Specific solvation interactions were also evident for SX in PEG 400 as demonstrated by the FTIR spectral

Table 5
Summary of the analysis of variance for the model equation of the median diameter of salmeterol xinafoate particles as a function of the crystallization variables

Source	Sum of squares	DF	Mean square	*F* value	$p > F$
Model	30.6429	4	7.66072	21.7414	<0.0001
Residual	1.24077	40	0.352356		
Lack of fit	12.8535	4	0.310192	0.868785	0.4921
Pure error	30.6429	36	0.357041		
Corrected total	44.7371	44			
Root mean square error		0.594	*R*-squared		0.685
Dependent mean		3.582	Adjusted *R*-squared		0.654
% Coefficient variance		16.574	Predicted *R*-squared		0.584
Predicted residual sum squares		18.613	Adequate precision		13.594

Table 6
Summary of the analysis of variance for the model equation of the cumulative 90% undersize diameter of salmeterol xinafoate particles as a function of the crystallization variables

Source	Sum of squares	DF	Mean square	*F* value	$p > F$
Model	2125.080	3	708.361	24.296	<0.0001
Residual	1195.380	41	29.156		
Lack of fit	870.991	5	174.198	19.332	<0.0001
Pure error	324.388	36	9.011		
Corrected total	3320.460	44			
Root mean square error		5.400	*R*-squared		0.640
Dependent mean		17.567	Adjusted *R*-squared		0.614
% Coefficient variance		30.738	Predicted *R*-squared		0.573
Predicted residual sum squares		1417.530	Adequate precision		13.982

changes. The hydroxyl peak broadening indicated the formation of intermolecular H-bonds and the ionic salt, SX [63]. The further spectral changes indicated a change in the polymer conformation which might have facilitated solvation [64] upon dissolution of SX.

The applicability of employing PEG as a solvent for the antisolvent micronization of hydrophobic compounds was shown by the ability to produce particles with a median diameter in the low micron size range (Table 1). The 2^4 factorial design was effective at screening the experimental factor space to provide an indication of the major effects of the crystallization operating parameters on the particle size of the crystallized particles. The four factors (drug concentration, PEG concentration, addition rate of antisolvent and stirring speed) accounted for the supersaturation of SX in the crystallizer, the rate of generation of supersaturation and the hydrodynamic conditions of the crystallizer, respectively, that affect PSD. Objective interpretation of effects from factorial design experiments relies on robust analysis of variance (ANOVA) and multiple linear regression analysis. The screening ability is strengthened by increasing the degrees of freedom, achieved by replicate measurement [65]. It was clear from the replicate crystallization of the centre points ($n = 3$) that greater variation in the principal outcome (median diameter) was attributable to the measurement of particle size, rather than the crystallization process. The variance in particle size measurements is generally determined by the sampling process [66]. Thus, to strengthen the experimental design, pseudo-replicates were introduced which involved replicate determinations of particle size ($n = 3$) rather than replicate manufacturing steps.

The 2^4 factorial study was suitable only for the general screening of effects, as a consequence of the curvature detected in the median diameter response. Two-level factorial design assumes linearity, and it was shown that greatest contribution to the mean square of variance for the model was attributed to the curvature, and hence, the significant lack of fit. A further complication in interpreting the effect of the operational conditions on the production of microparticles was the number of interacting terms. In accordance with classical nucleation theory [67] when supersaturation was increased (factors A, B and the two-way interactions AD, BD and BC) the median particle diameter decreased. A higher supersaturation leads to a large number of smaller crystals when supersaturation is consumed by nucleation events rather than crystal growth. The decrease in median particle diameter as the addition rate of the antisolvent (water) increased indicated that the extent of nucleation was not only determined by the maximal supersaturation, but also the rate and process of generation of supersaturation.

Classical nucleation theory relies on achieving rapid and homogeneous mixing of the crystallization solvents to ensure homogeneity of the level of supersaturation throughout the crystallizer. Thus the addition rate of the antisolvent and the hydrodynamic conditions of mixing obtaining in the crystallizer are crucial to this effect. Positive correlations between the median diameter and a number of factors were observed. These positive correlations

(indicating an increased median diameter at the upper factor levels) arose from the slower rate of generation of supersaturation due to a slower descent down the solubility curve (interactions AB and ABD). In addition the resultant particle size was affected by the hydrodynamic properties of the crystallizer, and both the efficiency and process of mixing the two solutions (C, D, ABD and AB). The high $D_{(v,0.9)}$ values in the majority of cases indicated a significant proportion of the particles would be unsuitable for inhaled drug delivery. However, the potential of the PEG solvent system for the controlled production of microparticles was shown by the relatively narrow PSD obtained for the centre point conditions (experiments 3, 10, and 14). Therefore, based on the predictable response of the median diameter to supersaturation, the centre point conditions were chosen to clarify the hydrodynamic effects on the particle size distribution to optimize microparticle production.

The use of a three-level factorial design (3^2) allowed the degree of curvature observed in the screening study to be taken into account. The statistical fit of the models was not ideal (only 65% and 61%, respectively, of the variance in the median and cumulative 90% undersize diameter could be described by the respective statistical models). A low correlation coefficient does not necessarily mean, however, that the model is not a reasonable description of the crystallization system from which inferences may be drawn on the controlling mechanisms [68].

The $D_{(v,0.5)}$ decreased with an increase in addition rate of the antisolvent while a curvature was seen in response to the stirring rate (Fig. 3). This can be interpreted by considering the response of the $D_{(v,0.9)}$ which increased as a linear function of stirrer speed (Fig. 4). Therefore any tendency to decrease the median diameter by increasing the stirring rate is opposed by a broadening of the PSD. Conversely an increase in the antisolvent addition rate decreased the median diameter, but a degree of curvature in the $D_{(v,0.9)}$ response indicated a broadening of the PSD. The addition rate of the antisolvent determines the rate of descent down the solubility curve and hence the rate of generation of supersaturation. The final PSD in a precipitation process is determined by the relative balance of the kinetic rates of nucleation and crystal growth. A high rate and degree of nucleation results in a smaller median particle diameter. The PSD, however, is dependent on the initial number of nuclei formed and also on the growth rate of those nuclei. The effective degree of supersaturation generated by a given mass of antisolvent is increased by increasing the addition rate [69] leading to extensive nucleation. However, both nucleation and growth increase in the presence of high supersaturation and hence slow addition of antisolvent result in a competition between fresh nucleation and growth of nuclei formed early in the precipitation process, leading to curvature in the $D_{(v,0.9)}$ response [70].

Ultimately nucleation is a process which occurs at the molecular level and for supersaturation to occur the PEG solution and the water antisolvent must be mixed at the molecular level by the process of micromixing [71]. However, PEG demonstrates a higher viscosity than most conventional solvents, and the difference in viscosity between PEG and water renders rapid homogeneous liquid mixing difficult [72]. The PEG–water system demonstrated a balance between micromixing and mesomixing (a larger scale mass transfer of the antisolvent). The lower rate of micromixing in viscous systems ensures a competition between micromixing and nucleation leading to a low nucleation rate at low antisolvent addition rates. Thus supersaturation can be consumed by crystal growth leading to higher particle sizes. As the antisolvent addition rate is increased, a shift in the balance of micro- to mesomixing occurs [73]. Mesomixing leads to localization of high levels of supersaturation in turbulent eddies and concomitant high rates of nucleation. Thus large numbers of primary nuclei are formed which possess a large surface area, and undergo limited growth in regions of lower local supersaturation leading to a narrow PSD.

Stirring also affects the balance of micro- and mesomixing processes. An increased stirrer speed increases the rate of micromixing enabling subsequent nucleation and the median particle size to be decreased. However, increased agitation minimizes local supersaturation (and lowers nucleation rates) by facilitating turbulent mesomixing. Crystal growth involves an element of volume-diffusion control where solute molecules must diffuse through a diffusion barrier around nascent crystals [67]. Increasing the stirring speed facilitates diffusion by decreasing the thickness of the stagnant boundary layer, hence affecting the balance between nucleation and crystal growth. Both of these reasons explain the curvature observed in the response surface of the median diameter as a function of stirrer speed.

5. Conclusions

PEG has been shown to be eminently suitable as a crystallization medium for the antisolvent crystallization of SX. A sufficient degree of solubilization for SX in water enabled the production of microparticles suitable for exploitation in topical lung drug delivery according to a novel and environmentally benign production method of amphiphilic crystallization. Crucially, the PSD was shown to depend on the hydrodynamic conditions prevailing in the crystallizer and did not require the use of traditional crystallization inhibitors. In this study the factors controlling the microcrystallization of SX by amphiphilic crystallization have been identified. Future work will focus on determining the suitability of the AmphiCrys process for other drug substances. Additionally the microcrystals will be characterized to determine their suitability for pulmonary delivery.

Acknowledgements

The authors acknowledge MedPharm Ltd. and King's College London for funding this work.

References

[1] M. Gumbleton, G. Taylor, Challenges and innovations in effective pulmonary systemic and macromolecular drug delivery, Adv. Drug Deliv. Rev. 58 (2006) 993–995.

[2] B. Forbes, C. Ehrhardt, Human respiratory epithelial cell culture for drug delivery applications, Eur. J. Pharm. Biopharm. 60 (2005) 193–205.

[3] M. Sakagami, In vivo, in vitro and ex vivo models to assess pulmonary absorption and disposition of inhaled therapeutics for systemic delivery, Adv. Drug Deliv. Rev. 58 (2006) 1030–1060.

[4] J.N. Pritchard, The influence of lung deposition on clinical response, J. Aerosol Med. 14 (2001) S19–S26.

[5] T. Crowder, A. Hickey, Powder specific active dispersion for generation of pharmaceutical aerosols, Int. J. Pharm. 327 (2006) 65–72.

[6] M. Rehman, B.Y. Shekunov, P. York, D. Lechuga-Ballesteros, D.P. Miller, T. Tan, P. Colthorpe, Optimisation of powders for pulmonary delivery using supercritical fluid technology, Eur. J. Pharm. Sci. 22 (2004) 1–17.

[7] H.K. Chan, N.Y.K. Chew, Novel alternative methods for the delivery of drugs for the treatment of asthma, Adv. Drug Deliv. Rev. 55 (2003) 793–805.

[8] R. Pauwels, S. Newman, L. Borgstrom, Airway deposition and airway effects of antiasthma drugs delivered from metered-dose inhalers, Eur. Respir. J. 10 (1997) 2127–2138.

[9] D. Price, M. Thomas, G. Mitchell, C. Niziol, R. Featherstone, Improvement of asthma control with a breath-actuated pressurised metred dose inhaler (BAI): a prescribing claims study of 5556 patients using a traditional pressurised metred dose inhaler (MDI) or a breath-actuated device, Respir. Med. 97 (2003) 12–19.

[10] U.H.U. Cegla, Pressure and inspiratory flow characteristics of dry powder inhalers, Respir. Med. 98 (2004) S22–S28.

[11] H.D.C. Smyth, The influence of formulation variables on the performance of alternative propellant-driven metered dose inhalers, Adv. Drug Deliv. Rev. 55 (2003) 807–828.

[12] H.K. Chan, Dry powder aerosol drug delivery-opportunities for colloid and surface scientists, Colloids Surf. A 284–285 (2006) 50–55.

[13] M. Tobyn, J.N. Staniforth, D. Morton, Q. Harmer, M.E. Newton, Active and intelligent inhaler device development, Int. J. Pharm. 277 (2004) 31–37.

[14] S.P. Newman, W.W. Busse, Evolution of dry powder inhaler design, formulation, and performance, Respir. Med. 96 (2002) 293–304.

[15] C.J. Musante, J.D. Schroeter, J.A. Rosati, T.M. Crowder, A.J. Hickey, T.B. Martonen, Factors affecting the deposition of inhaled porous drug particles, J. Pharm. Sci. 91 (2002) 1590–1600.

[16] A.A. Elamin, C. Ahlneck, G. Alderborn, C. Nystrom, Increased metastable solubility of milled griseofulvin, depending on the formation of a disordered surface structure, Int. J. Pharm. 111 (1994) 159–170.

[17] G.H. Ward, R.K. Schultz, Process-induced crystallinity changes in albuterol sulfate and its effect on powder physical stability, Pharm. Res. 12 (1995) 773–779.

[18] L. Mackin, R. Zanon, J.M. Park, K. Foster, H. Opalenik, M. Demonte, Quantification of low levels (<10%) of amorphous content in micronised active batches using dynamic vapour sorption and isothermal microcalorimetry, Int. J. Pharm. 231 (2002) 227–236.

[19] H. Steckel, N. Rasenack, P. Villax, B.W. Muller, In vitro characterization of jet-milled and in-situ-micronized fluticasone-17-propionate, Int. J. Pharm. 258 (2003) 65–75.

[20] A. Bauer-Brandl, Polymorphic transitions of cimetidine during manufacture of solid dosage forms, Int. J. Pharm. 140 (1996) 195–206.

[21] H.G. Brittain, Effects of mechanical processing on phase composition, J. Pharm. Sci. 91 (2002) 1573–1580.

[22] J.Y.Y. Heng, F. Thielmann, D.R. Williams, The effects of milling on the surface properties of form I paracetamol crystals, Pharm. Res. 23 (2006) 1918–1927.

[23] P. York, M.D. Ticehurst, J.C. Osborn, R.J. Roberts, R.C. Rowe, Characterisation of the surface energetics of milled DL-propranolol hydrochloride using inverse gas chromatography and molecular modelling, Int. J. Pharm. 174 (1998) 179–186.

[24] H.H.Y. Tong, B.Y. Shekunov, P. York, A.H.L. Chow, Influence of polymorphism on the surface energetics of salmeterol xinafoate crystallized from supercritical fluids, Pharm. Res. 19 (2002) 640–648.

[25] D. Cline, R. Dalby, Predicting the quality of powders for inhalation from surface energy and area, Pharm. Res. 19 (2002) 1274–1277.

[26] M. Davies, A. Brindley, X.Y. Chen, M. Marlow, S.W. Doughty, I. Shrubb, C.J. Roberts, Characterization of drug particle surface energetics and Young's modulus by atomic force microscopy and inverse gas chromatography, Pharm. Res. 22 (2005) 1158–1166.

[27] L. Mackin, S. Sartnurak, I. Thomas, S. Moore, The impact of low levels of amorphous material (<5%) on the blending characteristics of a direct compression formulation, Int. J. Pharm. 231 (2002) 213–226.

[28] D. Ticehurst, A. Basford, I. Dallman, M. Lukas, V. Marshall, G. Nichols, D. Smith, Characterisation of the influence of micronisation on the crystallinity and physical stability of revatropate hydrobromide, Int. J. Pharm. 193 (2000) 247–259.

[29] R.O. Williams, J. Brown, J. Liu, Influence of micronization method on the performance of a suspension triamcinolone acetonide pressurized metered-dose inhaler formulation, Pharm. Dev. Technol. 4 (1999) 167–179.

[30] E.M. Phillips, P.R. Byron, Surfactant promoted crystal growth of micronized methylprednisolone in trichloromonofluoromethane, Int. J. Pharm. 110 (1994) 9–19.

[31] H.H.Y. Tong, B.Y. Shekunov, P. York, A.H.L. Chow, Predicting the aerosol performance of dry powder inhalation formulations by interparticulate interaction analysis using inverse gas chromatography, J. Pharm. Sci. 95 (2006) 228–233.

[32] A.H.L. Chow, H.H.Y. Tong, P. Chattopadhyay, B.Y. Shekunov, Particle engineering for pulmonary drug delivery, Pharm. Res. 24 (2007) 411–437.

[33] H.H. Haberkorn, D. Franke, T. Frechen, W. Goesele, J. Rieger, Early stages of particle formation in precipitation reactions – quinacridone and boehmite as generic examples, J. Colloid Interface Sci. 259 (2003) 112–126.

[34] A. Mersmann, Crystallization and precipitation, Chem. Eng. Proc. 38 (1999) 345–353.

[35] T.L. Rogers, I.B. Gillespie, J.E. Hitt, K.L. Fransen, C.A. Crowl, C.J. Tucker, G.B. Kupperblatt, J.N. Becker, D.L. Wilson, C. Todd, E.J. Elder, Development and characterization of a scalable controlled precipitation process to enhance the dissolution of poorly water-soluble drugs, Pharm. Res. 21 (2004) 2048–2057.

[36] N. Rasenack, H. Steckel, B.W. Muller, Micronization of anti-inflammatory drugs for pulmonary delivery by a controlled crystallization process, J. Pharm. Sci. 92 (2003) 35–44.

[37] N. Rasenack, H. Steckel, B.W. Muller, Preparation of microcrystals by in situ micronization, Powder Technol. 143–144 (2004) 291–296.

[38] A.R. Ferrie, A.P. Savage, Novel apparatus and process for preparing crystalline particles, [WO0132125], United Kingdom, 2001.

[39] S.J. Brenek, D.J. Am Ende, Crystallization method and apparatus using an an impinging plate assembly, Pfizer Products Inc., [WO 2004047797], United States of America, 2006.

[40] R.W. Lancaster, H. Singh, A.L. Theophilus, Apparatus and process for preparing crystalline particles, Glaxo Group Limited (GB), [WO0038811], United Kingdom, 2001.

[41] J.S. Kaerger, R. Price, Processing of spherical crystalline particles via a novel solution atomization and crystallization by sonication (SAXS) technique, Pharm. Res. 21 (2004) 372–381.

[42] R. Thiering, F. Dehghani, N.R. Foster, Current issues relating to anti-solvent micronisation techniques and their extension to industrial scales, J. Supercrit. Fluids 21 (2001) 159–177.

[43] E. Rytting, K.A. Lentz, X.Q. Chen, F. Qian, S. Venkatesh, Aqueous and cosolvent solubility data for drug-like organic compounds, AAPS J. 7 (2005) E78–E105.

[44] J. Chen, S.K. Spear, J.G. Huddleston, R.D. Rogers, Polyethylene glycol and solutions of polyethylene glycol as green reaction media, Green Chem. 7 (2005) 64–82.
[45] Y.L. Huang, Q.B. Li, X. Deng, Y.H. Lu, X.K. Liao, M.Y. Hong, Y. Wang, Aerobic and anaerobic biodegradation of polyethylene glycols using sludge microbes, Process Biochem. 40 (2005) 207–211.
[46] Z. Moldovan, M.V. gado Luque, E.O. Salaverri, A. Suarez, R. Andreozzi, A. Insola, J.L. Martinez, Determination of polyethylene glycols in water by reversed-phase high-performance liquid chromatography, J. Chromatogr. A 723 (1996) 243–249.
[47] T. Arakawa, S.N. Timasheff, Mechanism of poly(ethylene glycol) interaction with proteins, Biochemistry (Mosc) 24 (1985) 6756–6762.
[48] M. Rito-Palomares, Practical application of aqueous two-phase partition to process development for the recovery of biological products, J. Chromatogr. B 807 (2004) 3–11.
[49] V.K. Sharma, D.S. Kalonia, Polyethylene glycol-induced precipitation of interferon alpha-2a followed by vacuum drying: development of a novel process for obtaining a dry, stable powder, AAPS Pharm. Sci. 6 (2004).
[50] X. Wang, C.S. Ponder, D.J. Kirwan, Low molecular weight poly(ethylene glycol) as an environmentally benign solvent for pharmaceutical crystallization and precipitation, Crys. Growth Des. 5 (2005) 85–92.
[51] A.F. Davis, J. Hadgraft, Effect of supersaturation on membrane transport: 1. Hydrocortisone acetate, Int. J. Pharm. 76 (1991) 1–8.
[52] S.L. Raghavan, K. Schuessel, A. Davis, J. Hadgraft, Formation and stabilisation of triclosan colloidal suspensions using supersaturated systems, Int. J. Pharm. 261 (2003) 153–158.
[53] E. Sjokvist, C. Nystrom, Physicochemical aspects of drug release. VI. Drug dissolution rate from solid particulate dispersions and the importance of carrier and drug particle properties, Int. J. Pharm. 47 (1988) 51–66.
[54] P. Lucas, K. Anderson, J.N. Staniforth, Protein deposition from dry powder inhalers: fine particle multiplets as performance modifiers, Pharm. Res. 15 (1998) 562–569.
[55] G. Brambilla, D. Ganderton, R. Garzia, D. Lewis, B. Meakin, P. Ventura, Modulation of aerosol clouds produced by pressurised inhalation aerosols, Int. J. Pharm. 186 (1999) 53–61.
[56] A. Wong, G.L. Briars, Acute pulmonary oedema complicating polyethylene glycol intestinal lavage, Arch. Dis. Child. 87 (2002) 537–538.
[57] K.W. Lu, H.W. Taeusch, B.E.N.G. Robertson, J.O.N. Goerke, J.A. Clements, Polymer-surfactant treatment of meconium-induced acute lung injury, Am. J. Respir. Crit. Care Med. 162 (2000) 623–628.
[58] D. Murnane, G.P. Martin, C. Marriott, Validation of a reverse-phase high performance liquid chromatographic method for concurrent assay of a weak base (salmeterol xinafoate) and a pharmacologically active steroid (fluticasone propionate), J. Pharm. Biomed. Anal. 40 (2006) 1149–1154.
[59] J.W. Millard, F.A. Alvarez-Nunez, S.H. Yalkowsky, Solubilization by cosolvents: establishing useful constants for the log-linear model, Int. J. Pharm. 245 (2002) 153–166.
[60] S.G. Machatha, S.H. Yalkowsky, Bilinear model for the prediction of drug solubility in ethanol/water mixtures, J. Pharm. Sci. 94 (2005) 2731–2734.
[61] T. Sato, H. Niwa, A. Chiba, R. Nozaki, Dynamical structure of oligo(ethylene glycol)s water solutions studied by time domain reflectometry, J. Chem. Phys. 108 (1998) 4138–4147.
[62] D. Sailaja, K.N. Raju, G.S.S. Devi, K. Subbarangaiah, Ultrasonic behaviour of aqueous solutions of polyethylene glycols on the temperature of adiabatic compressibility minimum of water, Eur. Polym. J. 34 (1998) 887–890.
[63] V. Di Noto, D. Longo, V. Munchow, Ion-oligomer interactions in poly(ethylene glycol)400/(LiCl)(x) electrolyte complexes, J. Phys. Chem. B 103 (1999) 2636–2646.
[64] R. Begum, H. Matsuura, Conformational properties of short poly(oxyethylene) chains in water studied by IR spectroscopy, J. Chem. Soc. Faraday Trans. 93 (1997) 3839–3848.
[65] N.A. Armstrong, K.C. James, in: N.A. Armstrong, K.C. James (Eds.), Factorial Design of Experiments, Taylor and Francis, London, UK, 1996, pp. 131–167.
[66] S.A. Lerke, S.A. Adams, Development and validation of a particle size distribution method for analysis of drug substance, Am. Pharm. Rev. (2002).
[67] N. Rodriguez-Hornedo, D. Murphy, Significance of controlling crystallization mechanisms and kinetics in pharmaceutical systems, J. Pharm. Sci. 88 (1999) 651–660.
[68] J. Sedzik, Regression analysis of factorially designed trials – a logical approach to protein crystallization, Biochim. Biophys. Acta 1251 (1995) 177–185.
[69] Z.Q. Yu, P.S. Chow, R.B.H. Tan, Application of attenuated total reflectance-Fourier transform infrared (ATR-FTIR) technique in the monitoring and control of anti-solvent crystallization, Ind. Eng. Chem. Res. 45 (2006) 438–444.
[70] J. Franke, A. Mersmann, The influence of the operational conditions on the precipitation process, Chem. Eng. Sci. 50 (1995) 1737–1753.
[71] J. Baldyga, W. Podgorska, R. Pohorecki, Mixing-precipitation model with application to double feed semibatch precipitation, Chem. Eng. Sci. 50 (1995) 1281–1300.
[72] X. Wang, J.M. Gillian, D.J. Kirwan, Quasi-emulsion precipitation of pharmaceuticals. 1. Conditions for formation and crystal nucleation and growth behavior, Crys. Growth Des. 6 (2006) 2214–2227.
[73] J. Baldyga, J.R. Bourne, S.J. Hearn, Interaction between chemical reactions and mixing on various scales, Chem. Eng. Sci. 52 (1997) 457–466.